Propagation of ultra-short, intense laser pulses in air

J. R. Peñano, P. Sprangle, B. Hafizi, A. Ting, D. F. Gordon, and C. A. Kapetanakos

Articles you may be interested in

Propagation of ultra-short, intense laser pulses in air[a]

J. R. Peñano,[b] P. Sprangle, B. Hafizi, A. Ting, D. F. Gordon, and C. A. Kapetanakos

Plasma Physics Division, Naval Research Laboratory, Washington, D.C. 20375

Recent theoretical, computational, and experimental work carried out at the Naval Research Laboratory on the propagation of ultra-short laser pulses in air is presented. Fully time-dependent, three-dimensional, nonlinear equations describing the propagation of laser pulses in air under the influence of diffraction, group velocity dispersion, Kerr nonlinearity, stimulated Raman scattering, ionization, and plasma wakefield excitation are presented and analyzed. The propagation code, HELCAP [P. Sprangle, J. R. Peñano, and B. Hafizi, Phys. Rev. E **66**, 046418 (2002)], is used to simulate the propagation of laser pulses in air under the influence of the physical processes mentioned above. Simulations of laser filamentation together with experimental measurements are used to confirm that the filamentation process is dependent on pulse duration. An equilibrium configuration for optical and plasma filaments in air is derived and the dynamic guiding and spectral broadening of a laser pulse is modeled. The effect of atmospheric turbulence on nonlinear self-focusing is demonstrated. Simulations of a recent electromagnetic pulse (EMP) generation experiment are also presented and the efficiency of EMP generation is determined and found to be extremely small. © *2004 American Institute of Physics.* [DOI: 10.1063/1.1648020]

I. INTRODUCTION

The propagation of ultra-short (~100 fs), intense (~10^{13}–10^{14} W/cm^2) laser pulses in the atmosphere is rich in nonlinear physics and may have a broad range of applications for remote sensing of chemical and biological agents, induced electrical discharges, and other directed energy applications. Experiments using terawatt pulses with durations less than a picosecond demonstrate the formation and long-distance propagation of plasma and optical filaments, white light generation, and emission of sub-THz electromagnetic pulses (EMP).[1–18]

The propagation characteristics of a laser pulse are determined by the refractive index of the propagation medium. For highly intense pulses with sub-picosecond durations, the refractive index is dependent on both the laser intensity and pulse duration. The optical Kerr effect is manifested by a nonlinear contribution to the refractive index that is proportional to the laser intensity and can lead to self-focusing. Stimulated rotational Raman scattering by the molecular constituents of air can lead to a delayed nonlinear response when the pulse duration is comparable with the molecular rotational period. Consequently, pulses that are short compared to the rotational period experience an effectively smaller nonlinear refractive index. The dependence of the nonlinear index on pulse duration affects the focusing and filamentation of the laser pulse as well as the subsequent guided propagation of the filaments.

These processes, along with the effects of diffraction, nonlinear self-focusing, ionization, and plasma defocusing play an important role in the guided propagation of laser and plasma filaments.[1,5,6,19–26] The optical Kerr effect, stimulated

Raman scattering, and ionization also contribute to considerable spectral broadening and efficient white light generation by the guided laser pulse.[8,9,23,27–32]

Recently, it has been observed that a broadband electromagnetic pulse (EMP) of terahertz radiation can be generated within the plasma filaments formed by an ultra-short (~100 fs), high-intensity (~10^{13}–10^{14} W/cm^2) laser pulse propagating in air.[17] The spatial gradients associated with the laser pulse envelope as well as electron collisions lead to ponderomotive forces on the plasma electrons. These forces cause the electrons to oscillate, setting up plasma currents. These induced plasma currents, which travel with the laser pulse, are the source of the EMP. The axial extent of the EMP is limited, and consequently, the spectrum of the EMP pulse can be broad.

In this paper, we report on several theoretical, computational, and experimental studies carried out at the Naval Research Laboratory (NRL) on the topics discussed above. Specifically, we examine the dependence of the filamentation process on pulse duration and model the dynamic guiding and spectral broadening of an optical/plasma filament. We then illustrate the effects of atmospheric turbulence on the propagation of these short pulses. In particular, in Ref. 33 we considered the possibility of generating a remote white light source by utilizing the nonlinear and dispersive properties of air to focus a laser pulse at kilometer distances. Over these distances, however, atmospheric turbulence can significantly distort the phase fronts of the laser pulse and disrupt the nonlinear self-focusing process. Here, we numerically determine an approximate turbulence threshold at which nonlinear self-focusing is prevented. Finally, we investigate EMP emission and determine the efficiency of converting laser energy into EMP energy for a recent experiment.[17]

The propagation code used throughout this study is HELCAP (High Energy Laser Code for Atmospheric Propa-
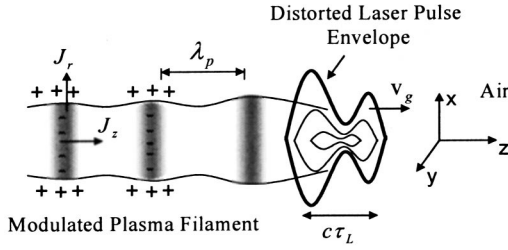
FIG. 1. Schematic diagram for atmospheric propagation and EMP generation showing the orientation of the coordinate axes, the laser pulse envelope, and the modulated plasma filament formed by the laser pulse. The laser pulse is guided and undergoes spectral broadening as discussed in the text. The ponderomotive forces associated with the laser pulse envelope drive radial and axial currents, J_r and J_z, respectively, which are the source of EMP. The filament is modulated at the plasma wavelength, λ_p. The axial EMP electric field outside the filament is small due to shielding by surface charges at the air-plasma boundary.

gation). HELCAP is a 4D (3D space+time) computer simulation developed at NRL which models the propagation of high-power laser pulses through air under the influence of a variety of linear and nonlinear processes. These processes include diffraction, dispersion, turbulence, nonlinear self-focusing, ionization, stimulated rotational Raman scattering, laser energy depletion due to ionization and collisions, thermal blooming, and quantum saturation. The code numerically solves propagation equations which determine the self-consistent evolution of the laser envelope and the surrounding air medium. In addition, a separate code, which solves the full Maxwell equations for the EMP field and a reduced set of propagation equations for the driving laser field, has been developed to model the generation of THz electromagnetic pulses in air.

This paper is organized as follows: The nonlinear propagation equations used in the HELCAP simulation are presented in Sec. II. A numerical and experimental illustration of the effects of pulse duration on the filamentation process is presented in Sec. III. Guiding and white light generation from an ionizing laser pulse is discussed in Sec. IV. The effects of atmospheric turbulence on pulse compression are investigated in Sec. V, and the generation of THz electromagnetic pulses and a simulation of a recent experiment are presented in Sec. VI. Section VII summarizes the results of our studies.

II. NONLINEAR PROPAGATION EQUATIONS

In deriving the propagation equation, it is assumed that the laser electric field, $\mathbf{E}(\mathbf{r},t)$, is a function of space and time and can be written in the form

$$\mathbf{E}(\mathbf{r},t) = A(\mathbf{r},t)\exp(i\psi(z,t))\hat{\mathbf{e}}_x/2 + \text{c.c.}, \qquad (1)$$

where $A(\mathbf{r},t)$ is a complex amplitude, $\mathbf{r} = x\hat{\mathbf{e}}_x + y\hat{\mathbf{e}}_y + z\hat{\mathbf{e}}_z$ denotes position in a Cartesian coordinate system defined by the unit vectors $(\hat{\mathbf{e}}_x, \hat{\mathbf{e}}_y, \hat{\mathbf{e}}_z)$, t denotes time, $\psi(z,t) = k_0 z - \omega_0 t$ is the phase, k_0 is the carrier wavenumber, ω_0 is the carrier frequency, and c.c. denotes the complex conjugate. A schematic diagram of the coordinate axes, laser pulse, plasma filament, and driven currents is shown in Fig. 1. The direction of propagation is along the z axis.

It proves useful to transform the independent variables from (z,t) to (z,τ), where $\tau = t - z/v_g$ and v_g is linear group velocity of the pulse. In this reference frame, the complex amplitude of the laser pulse evolves according to[33]

$$
\begin{aligned}
&\left[\nabla_\perp^2 - \frac{\omega_p^2}{c^2}(1 - i\nu_e/\omega_0) + 2ik_0\frac{\partial}{\partial z} - \frac{2}{\beta_g}\frac{\partial^2}{\partial z\partial c\tau} + \frac{\partial^2}{\partial z^2} \right.\\
&\left. \quad - c^2 k_0\beta_2\frac{\partial^2}{\partial c^2\tau^2} + i\alpha_3\frac{c}{\omega_0}\frac{\partial^3}{\partial c^3\tau^3} \right]A\\
&= -\left[\frac{2\omega_0^2}{c^2}n_0\delta n_T + \frac{\omega_0^2 n_0^2 n_K}{4\pi c}|A|^2 + \frac{\omega_p^2}{\omega_0^2}\frac{q^2|A|^2}{4m^2c^4} - \frac{\omega_p^2}{c^2}\frac{\delta n_e}{n_e} \right.\\
&\left. \quad + 8\pi ik_0\frac{U_{\text{ion}}}{|A|^2}\frac{\partial n_e}{\partial c\tau} + 4\pi\frac{\omega_0^2}{c^2}\chi_L Q(\mathbf{r},t) \right]A, \qquad (2)
\end{aligned}
$$

where $\nabla_\perp^2$ is the transverse Laplacian operator, $\omega_p(\mathbf{r},t) = (4\pi q^2 n_e(\mathbf{r},t)/m)^{1/2}$ is the plasma frequency, n_e is the plasma density generated by ionization as specified by Eq. (4), ν_e is the electron collision frequency, and $\beta_g = v_g/c$. The dispersion coefficients are denoted by $\beta_\ell = \partial^\ell\beta(\omega)/\partial\omega^\ell|_{\omega=\omega_0}$, where $\beta(\omega) = (\omega/c)[1 + 4\pi\hat{\chi}_L(\omega)]^{1/2} = (\omega/c)n_0(\omega)$, $n_0(\omega)$ is the linear refractive index and $\hat{\chi}_L(\omega)$ is the linear susceptibility. The group velocity dispersion (GVD) coefficient is denoted by β_2 and $\alpha_3 = -c^2\omega_0(\beta_1\beta_2 + \frac{1}{3}\beta_0\beta_3)$ is the effective third-order dispersion coefficient. The quantity δn_T is the perturbation to the refractive index due to atmospheric turbulence, n_K is the electronic contribution to the nonlinear refractive index, δn_e is the perturbed plasma density driven by the ponderomotive forces associated with the laser envelope, U_{ion} is the ionization energy, $\chi_L \equiv \hat{\chi}_L(\omega_0)$ is the linear susceptibility at the frequency ω_0, and Q is the response function for stimulated rotational Raman scattering. The term proportional to $\omega_p^2|A|^2$ leads to relativistic focusing. The term containing U_{ion} accounts for laser energy depletion due to ionization.

Stimulated Raman scattering can arise through the interaction of the laser with the dipole moments of the molecular constituents of air (principally N_2 and O_2). The interaction may be analyzed quantum mechanically using a three-level model.[34,35] The result of this analysis is a pair of equations for the Raman response function $Q(\mathbf{r},\tau)$ and the population inversion function $W(\tau)$ given by

$$\frac{\partial^2 Q}{\partial\tau^2} + \Omega_0^2 Q + 2\Gamma_2\frac{\partial Q}{\partial\tau} = -\frac{\mu^2}{\hbar^2}\frac{\omega_R}{\Omega}W|A|^2, \qquad (3a)$$

$$\frac{\partial W}{\partial\tau} = \frac{\mu^2/\hbar^2}{\omega_R\Omega}\left(\frac{\partial Q}{\partial\tau} + \Gamma_2 Q\right)|A|^2 - \Gamma_1(1+W), \qquad (3b)$$

where $\Omega_0^2 = \omega_R^2 + \Gamma_2^2$, ω_R is the fundamental rotational frequency, μ is the effective dipole moment, Γ_1 and Γ_2 are phenomenological damping rates (Γ_1 is the population relaxation rate and Γ_2 is the dipole dephasing rate) and $\Omega \equiv \Omega_{32} \approx \Omega_{31}$ is the frequency associated with transition from a higher energy virtual state (state 3) to one of two lower energy rotational states (states 1 and 2).

The free electron density in air can change because of ionization, recombination, and attachment processes. The rate equation for electron density n_e is

$$\frac{\partial n_e}{\partial t} = W_{ion} n_n - \eta n_e - \beta_r n_e^2, \tag{4}$$

where n_n is the neutral gas density, W_{ion} is the photoionization rate, η is the electron-attachment rate coefficient and β_r is the recombination coefficient. For the laser pulses of interest here, which have durations of ~ 1 ps or less, recombination and attachment processes play a negligible role in the propagation of a single pulse.[14] The ionization rate W_{ion} is an intensity dependent analytic function chosen to fit the experimentally measured short-pulse ionization rate reported in Refs. 25 and 36 and is valid in both the multiphoton and tunneling ionization regimes (see Ref. 37).

An electron, however, can absorb more photons than is necessary for multiphoton ionization. This process is referred to as above-threshold ionization (ATI).[38] In ATI, when the electron absorbs $s > \ell$, photons, it enters a continuum state with an excess energy of $(s - \ell)\hbar \omega_0$. This excess energy is manifested as oscillatory and ponderomotive motion of the ionized electron. Although the ATI process is inherently quantum mechanical, certain aspects have classical interpretations.[39] In our model, the energy depleted from the laser pulse due to the ATI process is accounted for classically, i.e., the enhanced energy gain of free electrons in the field of the laser is included, while the quantization of the electron energy is not.[33]

Thermal blooming effects are not important for the laser pulses considered here and are neglected. Our investigation of the thermal blooming of high average power beams is reported elsewhere.[40]

III. NONLINEAR FOCUSING AND FILAMENTATION

The growth rate and transverse wavenumber of the filamentation instability[41] is dependent on the ratio P_L/P_{NL}, where P_L is the laser power and P_{NL} is the effective nonlinear self-focusing power which is a function of the nonlinear refractive index and can contain both Kerr and Raman contributions. The nonlinear refractive index associated with Kerr and Raman nonlinearities is dependent on both the laser intensity and the pulse duration. Hence, the time dependence of the refractive index affects the filamentation process.

For illustrative purposes only, we consider the 1D limit, i.e., no transverse variation, in the following discussion of the refractive index. Writing the refractive index as a sum of linear and nonlinear parts, i.e., $n(\mathbf{r},\tau) = n_0 + \delta n(\mathbf{r},\tau)$, the nonlinear contribution due to Kerr and Raman effects is given by[35]

$$\delta n(z,\tau) \approx n_K I(z,\tau) + \frac{2\pi \chi_L}{n_0} Q(z,\tau), \tag{5}$$

where $I(z,\tau) = c n_0 |A(z,\tau)|^2/8\pi$ is the laser intensity.

In the limit $\Omega_R^2 \ll \Omega \Omega_0$, where $\Omega_R = \mu A_0/\hbar$ is the Rabi frequency associated with the peak electric field amplitude, A_0, the population inversion associated with stimulated Ra-

man scattering can be neglected, i.e., $W \approx -1$, and the Raman response function, from solving Eq. (3a), is given by[35]

$$Q(z,\tau) = \frac{\mu^2}{\hbar^2} \frac{1}{\Omega} \int_0^{\tau} d\tau' \, \exp[-\Gamma_2(\tau-\tau')]$$

$$\times \sin(\omega_R(\tau-\tau')) |A(z,\tau')|^2. \tag{6}$$

The Kerr and Raman terms are both proportional to laser intensity and contribute to the nonlinear refractive index at the same order. However, the Raman contribution represents a delayed nonlinear response that can be neglected for sufficiently short pulses, thus resulting in an effectively lower nonlinear index for short pulses.[35]

As an example, consider a constant amplitude laser pulse with duration τ_L. The field amplitude can be written as $A = A_0(\Theta(\tau) - \Theta(\tau-\tau_L))$, where $\tau = t - z/c$. From Eqs. (5) and (6), the nonlinear index within the pulse, i.e., $0 < \tau < \tau_L$, is $\delta n = n_{NL} I$ where the effective coefficient of nonlinearity is given by

$$n_{NL} = n_K + n_R[1 - e^{-\Gamma_2 \tau}(\cos(\omega_R \tau) + (\Gamma_2/\omega_R)\sin(\omega_R \tau))], \tag{7}$$

with

$$n_R = (4\pi/n_0)^2 \chi_L \frac{\omega_R}{\Omega} \frac{\mu^2}{\hbar^2 \Omega_0^2 c}. \tag{8}$$

In the long pulse limit ($\tau \gg 1/\Gamma_2$), the total nonlinear coefficient is given by $n_{NL} = n_K + n_R$, i.e., n_R represents the effective coefficient of nonlinearity due to Raman effects. In this parameter regime, the effective nonlinear focusing power is given by $P_{NL} = \lambda^2/[2\pi(n_K + n_R)n_0]$. For pulses short compared with the characteristic Raman times ($\tau \ll 1/\omega_R$, $\tau \ll 1/\Gamma_2$), the nonlinear refractive index is due to purely the bound electron response, i.e., $n_{NL} = n_K$, and is smaller than the nonlinear index associated with longer pulses.

The effect of the time dependence of the nonlinear refractive index on the filamentation process was verified experimentally and through simulations. In the experiment, a laser pulse with $\lambda = 0.8$ μm, spot size $R_0 \approx 4$ mm, and $P = 0.2$ TW was propagated ~ 10 m through air and its cross sectional image was recorded on burn paper. The pulse duration was varied from 120 to 180 fs keeping the pulse power constant. The burn paper images for these two cases are shown in Fig. 2. For the case of the 120 fs pulse, one filament is formed, while the 180 fs pulse shows the formation of multiple filaments. The higher degree of filamentation is consistent with the fact that the nonlinear refractive index of a longer pulse is larger due to Raman effects.

The experimental result was verified with simulations. For the simulations, the Raman and Kerr parameters for air are taken to be $\omega_R = 16 \times 10^{12}$ s^{-1}, $\Gamma_2 = 1.3 \times 10^{13}$ s^{-1}, and $n_K = n_R = 3 \times 10^{-19}$ cm^2/W. Choosing $n_K = n_R$ is consistent with experimental findings reported in Ref. 42. The GVD parameter $\beta_2 = 2.2 \times 10^{-31}$ s^2/cm and higher order dispersion has been neglected. The laser parameters used in the simulation were identical to those of the experiment. The initial fluence profile of the 120 fs laser pulse measured in the ex-
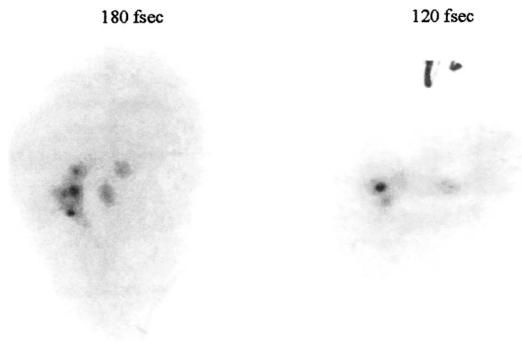
180 fsec   120 fsec

FIG. 2. Images of a 180 and 120 fs laser pulse recorded on burn paper after propagating ~11 m in air. The laser pulse had wavelength $\lambda = 0.8$ μm and spot size $R_0 \approx 4$ mm. The laser power in both cases was ~0.2 TW. It was observed that the longer duration pulse formed a larger number of filaments than the shorter duration pulse.

periment was digitized for use as input to the simulations. The longitudinal envelope of the laser pulse was assumed to be Gaussian, i.e., $A \sim \exp(-\tau^2/T_0^2)$. The laser intensity over the course of the simulation was sufficiently low that ionization was negligible.

Figure 3 shows the fluence distribution obtained from the simulation for pulses with full-width-half-maximum (FWHM) intensity durations of 120 and 180 fs after propagating ~1 m in air. The plots show the onset of the filamentation instability. Consistent with the experimental finding, the 120 fs pulse shows the formation of one main filament, while the 180 fs pulse shows multiple filaments.

IV. GUIDING AND SUPERCONTINUUM GENERATION

In this section, the long range propagation of an ionizing laser filament in air is considered. The propagation distance of a laser pulse in air is limited by a number of processes. Two fundamental laser pulse propagation mechanisms that can, in principle, result in extended propagation distances are (i) moving foci and (ii) self-guiding. In the moving foci mechanism the focal length depends on laser power through the optical Kerr effect and different temporal slices of the laser pulse focus at different distances.[43,44] This can give the illusion of extended propagation. However, only an infinitesimal fraction of the laser energy is propagated over

extended distances. In the self-guiding mechanism extended propagation distances can be obtained by balancing the defocusing effects of diffraction and plasma formation against nonlinear self-focusing, i.e., the Kerr effect. In self-guiding, losses such as ionization can deplete the laser pulse energy and significantly limit the propagation distance, as shown below.

The process of ionization and optical filament propagation can be analyzed by retaining diffraction, the nonlinear Kerr effect, plasma effects, collisional losses, and laser pulse energy depletion due to ionization in Eq. (2), i.e.,

$$\frac{\partial A}{\partial z} = \frac{i}{2}\frac{c}{\omega_0}\left(\nabla_\perp^2 + \frac{\omega_0^2 n_K}{4\pi c}\frac{n_n}{n_{n0}}|A|^2 - \frac{\omega_p^2}{c^2}\left(1 - i\frac{\nu_e}{\omega_0}\right)\right.$$

$$\left. + 8\pi i\frac{\omega_0}{c^2}\frac{U_{\text{ion}}}{|E_L|^2}\frac{\partial n_e}{\partial \tau}\right)A, \tag{9}$$

where n_{n0} is the ambient neutral density. The on-axis electron density is assumed to be generated by multiphoton ionization and is given by

$$\frac{\partial n_{e0}}{\partial \tau} = W_{mp}(r=0)n_n = \frac{2\pi\omega_0}{(\ell-1)!}\left(\frac{I(r=0)}{I_{mp}}\right)^\ell n_n, \tag{10}$$

where the integer $\ell \leqslant \text{Int}(U_{\text{ion}}/\hbar\omega_0 + 1)$ refers to the effective number of photons absorbed by the molecule in the ionization process, and U_{ion} is the ionization energy. Here, $I_{MP} \sim 10^{14}$ W/cm^2 and $\ell = 8$ are used to approximate the empirically determined ionization rate for ~100 fs laser pulses.[25,36]

Equation (9) can be approximately solved by employing the source dependent expansion (SDE) method.[45] In this method the laser field is assumed to have a Gaussian transverse profile
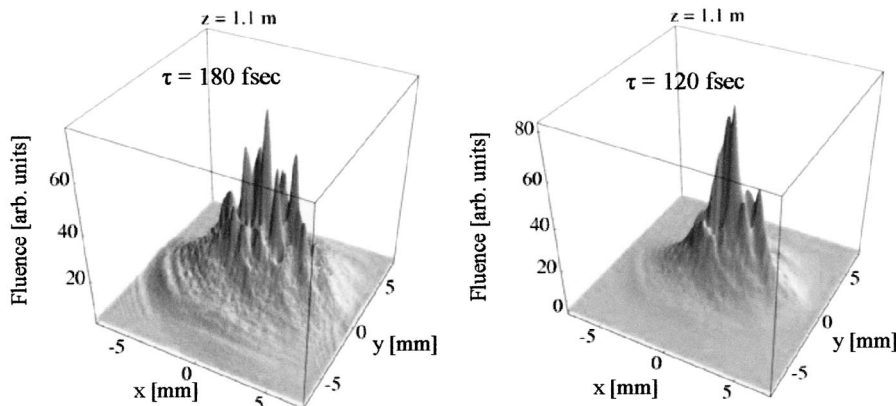
$$|A| = |A_0(z,\tau)|\exp[-r^2/R^2(z,\tau)], \tag{11}$$

FIG. 3. Spatial distributions of fluence obtained from the HELCAP simulation for a 120 fs pulse and a 180 fs pulse after propagating ~1 m in air. Simulation parameters for the laser are the same as those of the experimental result shown in Fig. 2. The laser power is 0.2 TW for both cases. The initial transverse intensity profile used in the simulation was obtained from a digitized experimental image of the 120 fs laser pulse. Note the larger number of filaments for the longer duration pulse.

where R is the laser spot size. For the Gaussian transverse profile the laser power is

$$P_L(z,\tau) = c|A_0(\tau)|^2 R^2(z,\tau)/16. \tag{12}$$

Employing the SDE method results in coupled equations for the spot size and power,

$$\frac{\partial^2 R(z,\tau)}{\partial z^2} - \frac{4c^2}{\omega_0^2}\frac{1}{R^3(z,\tau)}\left(1 - \frac{P_L(z,\tau)}{P_K}\right.$$
$$\left. + \frac{2\pi\ell r_e n_{e0}(0,z,\tau)}{(\ell+1)^2}R^2(z,\tau)\right) = W(z,\tau), \tag{13a}$$

$$\frac{\partial P_L(z,\tau)}{\partial z} = -\frac{1}{\ell+1}\frac{\omega_{p0}^2(0,z,\tau)}{\omega_0^2}\frac{\nu_e}{c}P_L(z,\tau)$$
$$-\frac{\pi}{2\ell}U_{\text{ion}}\nu_{\text{ion}}n_n R^2(z,\tau), \tag{13b}$$

where $P_K = \lambda_0^2/(2\pi n_K n_n/n_{n0})$ is the nonlinear Kerr focusing power, n_n is the neutral density, n_{n0} is the ambient neutral density, $r_e = q^2/mc^2$ is the classical electron radius and

$$W(z,\tau) = -\frac{1}{R}\left(\frac{\partial}{\partial z}(R^2 U) + R^2 U^2\right), \tag{13c}$$

$$U(z,\tau) = \frac{(\ell-1)}{2\ell}\frac{1}{P_L}\frac{\partial P_L}{\partial z} - \frac{1}{2\ell(\ell+1)^2}\frac{\omega_{p0}^2}{\omega_0^2}\frac{\nu_e}{c}. \tag{13d}$$

An approximate equilibrium of the filament's spot size can be found when the energy depletion due to ionization is low. Neglecting ionization on the right hand side of Eq. (13a) and taking $\partial R/\partial z = 0$, we obtain

$$P_{\text{eq}}(\tau) = P_{NL}\left(1 + \frac{2\pi\ell}{(\ell+1)^2}r_e R_{\text{eq}}^2(\tau)n_{e0}(\tau)\right), \tag{14}$$

where the subscript eq denotes the equilibrium value. This equilibrium condition assumes that the transverse profile of the laser pulse and plasma density remain Gaussian. In reality, the laser pulse becomes highly distorted transversely due to nonlinear focusing and longitudinally due to dispersion as shown in the simulation example below. In addition, energy loss due to collisions and ionization play a significant role.

Rewriting Eq. (13b), the decrease in the total laser pulse power as a function of propagation distance due to both collisional absorption and ionization is given by

$$\frac{\partial P_L(z,\tau)}{\partial z} = -\left(\frac{1}{L_{\text{coll}}} + \frac{1}{L_{\text{ion}}}\right)P_L(z,\tau), \tag{15a}$$

where

$$L_{\text{coll}} = (\ell+1)\frac{\omega_0^2}{\omega_{p0}^2}\frac{c}{\nu_e}, \tag{15b}$$

is the absorption length due to collisional effects and

$$L_{\text{ion}} = \frac{2\ell}{\pi}\frac{P_L}{U_{\text{ion}}\nu_{\text{ion}}n_n R^2}, \tag{15c}$$

is the absorption length due to ionization effects. It should be noted that due to the nonlinear character of Eq. (15a), the expressions in Eqs. (15b) and (15c) are at best local estimates for the scale lengths.

As an example, consider the case of a laser pulse having a power $P_L = 0.1$ TW, wavelength $\lambda_0 = 0.8\,\mu m$, pulse duration $\tau_L = 100$ fs, intensity $I_L = 5\times10^{13}$ W/cm^2 and spot size $R\sim360\,\mu m$, propagating in air with a neutral density $n_{n0} = 2.7\times10^{19}$ cm^{-3}, effective ionization energy of $U_{\text{ion}} = 8$ eV ($\ell=8$) and electron collision frequency of $\nu_e = \nu_{en} + \nu_{ei}\approx6\times10^{12}$ s^{-1}. In this case the ionization rate is $\nu_{\text{ion}}\sim10^{10}$ s^{-1} ($I_{MP}=10^{14}$ W/cm^2) and the electron density is $n_e\sim3\times10^{16}$ cm^{-3}, ($\omega_0/\omega_{p0}\sim230$). For these parameters the collisional absorption length is $L_{\text{coll}}\sim25$ m while the ionization absorption length is $L_{\text{ion}}\sim10$ m. It should be stressed that these characteristic scale lengths are very sensitive functions of the laser and plasma parameters.

The nonlinear interaction of an intense, short laser pulse in the atmosphere can result in significant spectral broadening due to self phase modulation. The phase of the laser field becomes modulated through the time dependent refractive index by nonlinear effects, ionization, Raman processes, etc. Although 3D effects also play an important role in spectral broadening a 1D analysis is useful. In 1D, it can be shown from Eq. (2) that the instantaneous frequency spread due to Kerr, Raman, and plasma effects is given by[33]

$$\delta\omega(z,\tau) = \left(-n_K\frac{\partial I}{\partial\tau} + n_R\int_0^\tau d\tau' W(\tau')\right.$$
$$\left.\times\frac{\partial R(\tau-\tau')}{\partial\tau}I(\mathbf{r},\tau') + \frac{1}{2n_0\omega_0^2}\frac{\partial\omega_p^2}{\partial\tau}\right)\frac{\omega_0 z}{c}, \tag{16a}$$

where

$$R(\tau) = \left(\frac{\omega_R^2 + \Gamma_2^2}{\omega_R}\right)e^{-\Gamma_2\tau}\sin(\omega_R\tau). \tag{16b}$$

Note that only the nonlinear terms in the refractive index will create new frequencies, the linear terms redistribute the frequencies within the pulse. The Kerr nonlinearity produces a red shift at the front of the pulse and a blue shift at the back while ionization produces a blue shift across the entire pulse. Stimulated Raman scattering, depending on the pulse duration, can produce both red and blue shifts. The frequency spread due to nonlinear effects increases linearly with the propagation distance.

The guiding and frequency broadening of an ultra-short laser pulse are illustrated in the following simulation example. A laser pulse with $\lambda=0.8\,\mu m$, $P=2.5$ GW is propagated in air. The initial laser envelope is given by $A(r,\tau,z=0) = A_0\exp(-r^2/R_0^2)\sin(\pi\tau/T_0)$ for $0<\tau<T_0$ and zero otherwise. The initial spot size and pulse duration are $R_0 = 54\,\mu m$ and $T_0 = 100$ fs, respectively.

In the simulation, the laser pulse envelope is seen to undergo a dynamic evolution characterized by an initial strong defocusing of the back of the laser pulse due to the generation of a plasma column and subsequent refocusing as
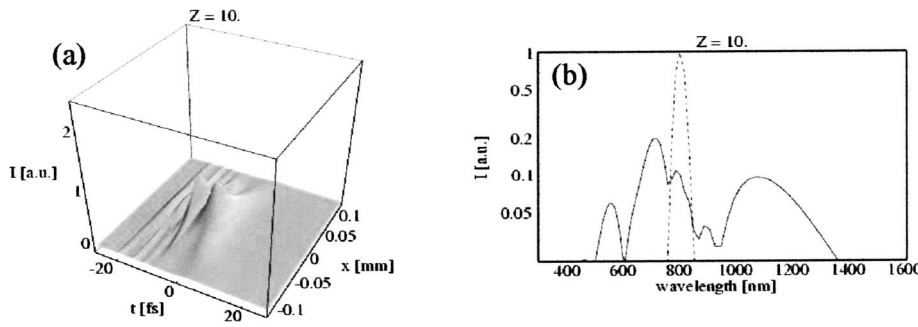
FIG. 4. (a) Laser intensity vs t and x (at $y=0$) after propagating $z=10\,Z_R$ in air. (b) On-axis laser spectrum at $z=0$ (dashed curve) and at $z=10\,Z_R$ (solid curve). The initial laser pulse has $\lambda=0.8$ μm, $P=2.5$ GW, $R_0=54$ μm, and $T_0=100$ fs.

the pulse shortens and the plasma density drops. The defocusing and refocusing occur several times and result in a dynamic guiding of the laser pulse for $\sim 10Z_R$, where $Z_R=k_0R_0^2/2$ is the Rayleigh length. In earlier works it was proposed that these recurrences underlie the experimentally observed long distance propagation of intense pulses in air.[24]

The intensity distribution after propagating $10Z_R$ is shown in Fig. 4(a). In the figure, $\tau=0$ marks the initial midpoint of the pulse. The leading edge of the pulse (-20 fs $<\tau<-10$ fs) where $P_L<P_{NL}$ has diffracted considerably while the middle portion of the pulse remains guided. Note that plasma defocusing of the back of the pulse has resulted in a much shorter laser pulse (~ 10 fs). The initial ($z=0$) and final ($z=10\,Z_R$) on-axis spectra are shown in Fig. 4(b). It is seen that the spectrum has broadened significantly and extends through the visible regime, i.e., white light is generated. The limited resolution of the simulation prevented further propagation.

V. NONLINEAR SELF-FOCUSING IN A TURBULENT ATMOSPHERE

In Ref. 33, it was proposed that a remote spark could be generated in the atmosphere by using the dispersive and nonlinear properties of air to simultaneously compress and focus an appropriately chirped laser pulse, thus ionizing the air and producing white light kilometers from the laser source. Because of the long range of propagation, the laser pulse can be affected by atmospheric turbulence. In this section, we numerically investigate the effects of turbulence on the nonlinear self-focusing process.

Turbulence is modeled numerically by employing a standard phase screen approach.[46] The turbulence spectrum is characterized by a modified von Kármán distribution[47] with index structure constant C_n^2 and inner and out scale lengths 1 cm and 100 m, respectively. The index structure constant is a measure of the strength of the turbulence. For example, weak and strong turbulence is characterized by $C_n^2\sim 10^{-17}\,\mathrm{m}^{-2/3}$ and $C_n^2\sim 10^{-13}\,\mathrm{m}^{-2/3}$, respectively.

The initial laser envelope is given by

$$A(r,\tau,z=0)=A_0\exp(-r^2/R_0^2)\exp[-(1+i\alpha_c)\tau^2/T_0^2],$$

with spot size $R_0=54$ μm, duration $T_0=100$ fs, and chirp parameter $\alpha_c=-20$. The value of the negative chirp is chosen so that the nonlinear transverse focal length and longitudinal compression length are equal. The chirp parameter α_c is related to the full Fourier spectral width at $1/e$ of the amplitude by $\Delta\omega=4(1+\alpha_c^2)^{1/2}/T_0$. The initial laser wavelength and peak intensity are $\lambda=0.8$ μm and $I_0=1$ GW/cm^2, respectively. These parameters are similar to the chirped pulse compression example discussed in Ref. 33. The laser pulse is propagated through air with varying degrees of turbulence. Figure 5 plots the peak fluence as a function of propagation distance for $C_n^2=0$, $C_n^2\sim 10^{-15}\,\mathrm{m}^{-2/3}$ (moderate turbulence), and $C_n^2\sim 10^{-13}\,\mathrm{m}^{-2/3}$ (strong turbulence). In the absence of turbulence, the laser focuses at a range of ~ 400 m. For $C_n^2\sim 10^{-15}\,\mathrm{m}^{-2/3}$, a well defined focal point occurs, but at a longer range (~ 450 m). In the presence of strong turbulence, $C_n^2\sim 10^{-13}\,\mathrm{m}^{-2/3}$, focusing does not occur.

The laser intensity cross section near focus, plotted in Fig. 6, shows that for $C_n^2=0$, the pulse focuses to a single filament on axis. For $C_n^2\sim 10^{-15}\,\mathrm{m}^{-2/3}$, a single filament is also formed, but it is slightly displaced (~ 3 mm) from the axis.

VI. GENERATION OF THz ELECTROMAGNETIC PULSES

In this section, we simulate the EMP produced by the interaction of ultrashort laser pulses with air and determine the conversion efficiency of laser pulse energy to the EMP. We have recently analyzed the generation of EMP from the propagation of intense laser pulses in air.[48] The results of our analysis can be summarized as follows: For steady state propagation, in which the laser pulse and plasma filament are static in the group velocity frame of the laser pulse, the
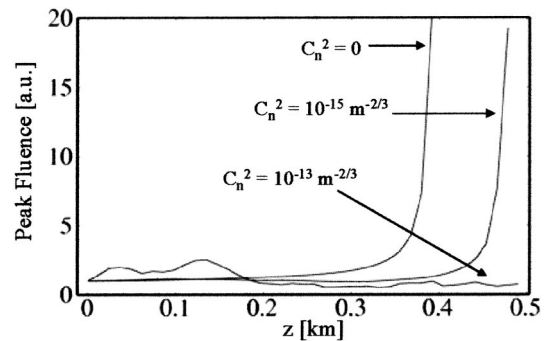

FIG. 5. Peak fluence of a chirped laser pulse vs propagation distance for propagation in air with varying degrees of turbulence. The initial laser pulse is characterized by $\lambda=0.8$ μm, $I_0=1$ GW/cm^2, $R_0=54$ μm, $T_0=100$ fs, and $\alpha_c=-20$ as defined in the text. Note the absence of nonlinear self-focusing in the presence of strong turbulence, i.e., $C_n^2=10^{-13}\,\mathrm{m}^{-2/3}$.
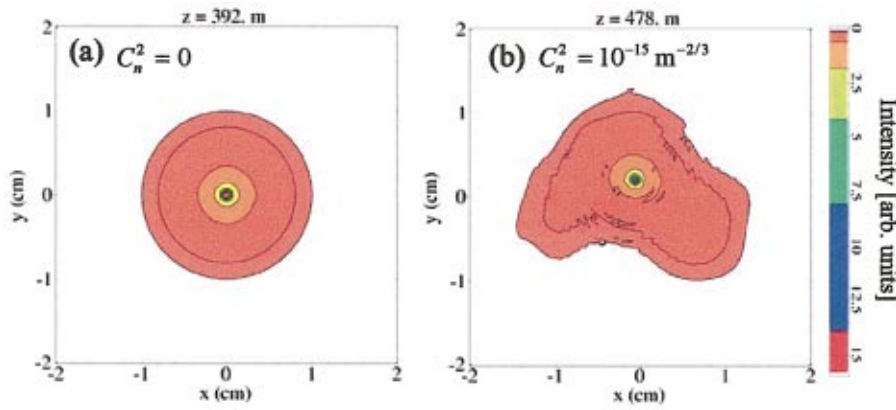
FIG. 6. (Color) Cross sections of laser intensity near focus for (a) $C_n^2=0$ and (b) $C_n^2=10^{-15}$ m$^{-2/3}$ corresponding to the simulations of Fig. 5.

plasma current source travels with a velocity equal to the laser pulse group velocity. Since the group velocity is necessarily less than the speed of light, there is no radiative EMP generated. The absence of radial EMP emission in the steady state is one of several fundamental differences between our results and those of Refs. 49. The absence of EMP in the steady state is analogous to the lack of Cherenkov radiation when the velocity of a charged particle is less than the velocity of light in the medium.[50] Under conditions of non-steady state (transient) propagation, the plasma currents can generate EMP having a radial energy flux. For nonsteady state pulse propagation, the plasma currents can have Fourier components with phase velocities greater than the laser pulse group velocity. These Fourier components can generate radiative EMP, analogous to Cherenkov radiation.

The wave equation for the EMP electric field $\mathbf{E}_{EMP}$ in air which is driven by plasma currents is given by

$$\nabla\times\nabla\times\mathbf{E}_{EMP}+\frac{n_0^2}{c^2}\frac{\partial^2\mathbf{E}_{EMP}}{\partial t^2}=-\frac{4\pi}{c^2}\frac{\partial\mathbf{J}}{\partial t}. \qquad (17)$$

The plasma currents are driven by the poderomotive forces associated with collisions and the spatial gradient of the laser envelope, i.e.,

$$\frac{\partial\mathbf{J}}{\partial t}+\nu_e\mathbf{J}=\frac{\omega_p^2}{4\pi}\mathbf{E}+\mathbf{S}, \qquad (18)$$

where the longitudinal and transverse components of the source term are given by

$$S_z\approx-\frac{q}{16\pi m}\frac{\omega_p^2}{\omega_0^2}\left(\frac{\partial}{\partial z}-\frac{2\nu_e}{c}-\frac{2}{c\omega_p^2}\frac{\partial\omega_p^2}{\partial t}\right)|A|^2 \qquad (19a)$$

and

$$\mathbf{S}_\perp\approx-\frac{q}{8\pi m}\frac{\omega_p^2}{\omega_0^2}\left(\frac{\partial}{\partial r}+\frac{1}{\omega_p^2}\frac{\partial\omega_p^2}{\partial r}\right)|A|^2\hat{\mathbf{e}}_r. \qquad (19b)$$

In writing Eqs. (19), axial symmetry is assumed and the axially symmetric circularly polarized laser field has the form $\mathbf{E}=A\exp(i(k_0z-\omega_0t))(\hat{\mathbf{e}}_x-i\hat{\mathbf{e}}_y)/2+$c.c. To obtain the ponderomotive source term self consistently, an equation de-
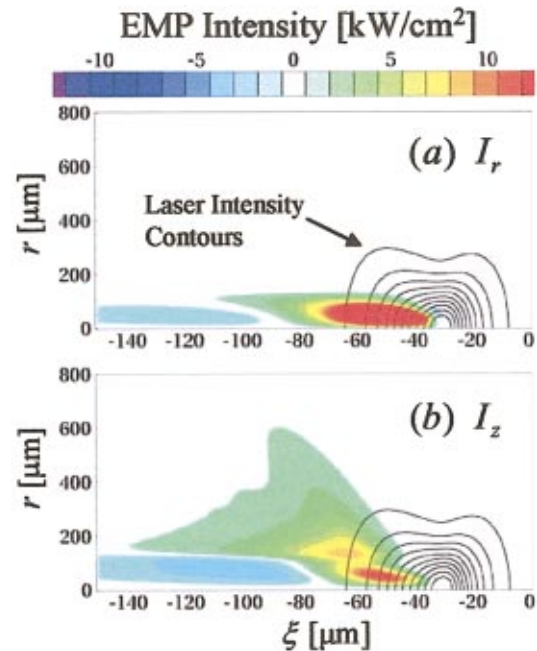
FIG. 8. (Color) Contours of (a) radial and (b) axial EMP radiance as a function of $\xi=z-\mathbf{v}_gt$ and radial position, r, at propagation distance $\Delta z=10$ cm. Unshaded contours indicate the laser intensity distribution. Initial ($z=0$) laser parameters for the simulation are $\lambda_0=0.8$ μm, $P_L=83$ GW, $\tau_L=120$ fs (FWHM), and $R_0=7.5$ mm. Parameters for air are taken to be $n_0-1=2.7\times10^{-4}$, $n_K=3\times10^{-19}$ cm^2/W, $U_{ion}=12$ eV, $\ell=8$, and $I_{MP}\sim10^{14}$ W/cm^2.
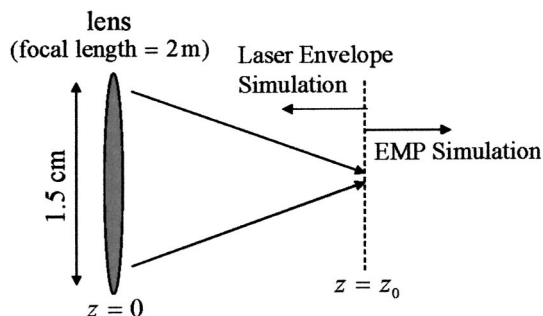

FIG. 7. Schematic diagram of the simulation of the EMP experiment of Ref. 17. The laser envelope simulation (without EMP) is performed from $z=0$ to $z=z_0$, where $z_0=1.82$ m. The full EMP simulation is carried out for $z>z_0$.
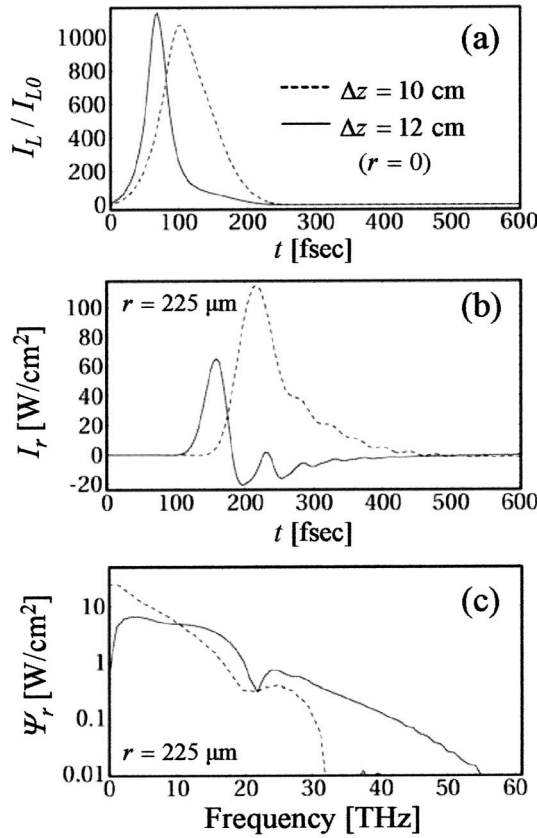
FIG. 9. (a) Normalized on-axis laser intensity vs time, (b) radial EMP Poynting flux, I_r, at radial position $r = 225$ μm vs time, and (c) corresponding temporal Fourier transform of I_r for propagation distances $\Delta z = 10$ cm (dashed curve) and 12 cm (solid curve). The radial position $r = 225$ μm is outside of the plasma filament. Simulation parameters correspond to those listed for Fig. 8.

scribing the evolution of the driving laser pulse is needed. Here, we use the SDE method, i.e., Eqs. (13), to solve for the evolution of the spot size and power of the Gaussian laser pulse.

The numerical simulations presented here are based on solving Eq. (17) for the EMP field, with the plasma current and source given by Eqs. (18) and (19). The laser envelope evolves according to Eqs. (13) and the plasma density is given by Eq. (4) with the assumption of multi-photon ionization.

The simulations are initialized at $t=0$ with the laser pulse propagating in vacuum in the positive z direction. The leading edge of the laser pulse at $t=0$ is located at axial position $z=0$. In the vacuum–air transition region from $z=0$ to $z=L_n$, the neutral density increases with the functional form

$$n_n(z) = n_{n0} \begin{cases} 1, & z \geq L_n \\ [10(z/L_n)^3 - 15(z/L_n)^4 + 6(z/L_n)^5], & z \leq L_n \end{cases},$$

and has the constant value $n_{n0} = 2.7 \times 10^{19}$ cm^{-3} for $z > L_n$.

A recent experiment reported in Ref. 17, measured an EMP from a femtosecond laser pulse propagating in air. In the experiment, a laser pulse with a FWHM duration of 120 fs, wavelength $\lambda_0 = 0.8$ μm, and energy ~ 30 mJ was passed

through an aperture of diameter 1.5 cm and focused into the air with a 2 m focal length lens. As the laser pulse focused and the intensity increased, a plasma filament was formed near the focal region and EMP was measured along the length of the plasma filament. The following results are from a simulation with similar parameters.

In our simulation, the parameters for air are taken to be $n_0 - 1 = 2.7 \times 10^{-4}$, $n_K = 3 \times 10^{-19}$ cm^2/W, $U_{ion} = 12$ eV, $\ell = 8$, $I_{MP} = 10^{14}$ W/cm^2, and $n_{n0} = 2.7 \times 10^{19}$ cm^{-3}. The laser pulse envelope is taken to be Gaussian in the transverse direction with a spot size $R_0 = 7.5$ mm. The longitudinal laser field profile is given by $|A(0,z,\tau)| = \hat{A}(z)\sin(\pi\tau/\tau_L)$, with $\tau_L = 240$ fs, which corresponds to a FWHM intensity duration of 120 fs. The laser pulse has wavelength $\lambda_0 = 0.8$ μm, peak power $P_L = 83$ GW, and energy ~ 10 mJ. The simulation is performed in two parts as illustrated in Fig. 7. The first part models the focusing of the initially low intensity laser pulse in air by a lens with a focal length of 2 m. Here the simulation covers a range $0 < z < z_0$, where $z_0 = 1.82$ m. Over this range, the laser intensity is sufficiently low that no appreciable plasma density is formed and no EMP is generated. To expedite the simulation, only the propagation equations for the driving laser pulse envelope are solved for $z < z_0$. The laser pulse envelope at $z = z_0$ is used to initialize the full-scale EMP simulation for $z > z_0$.

The spatial distribution of the radial EMP Poynting flux, I_r, and axial EMP Poynting flux, I_z, are shown in Figs. 8(a) and 8(b), respectively, at $\Delta z \sim 10$ cm where they achieve their maximum values. Inside the plasma filament, the Poynting fluxes are peaked within the laser pulse and decay in amplitude behind the pulse. The radial flux is mainly confined within the plasma filament while the axial flux extends radially beyond the filament. Although not apparent from the color scale of the plot, a small radial flux is present outside of the filament which can be experimentally detected.

Figure 9(a) plots the on axis laser intensity (normalized to its peak value at $z = 0$) versus time at $\Delta z = 10$ cm (dashed curve) and $\Delta z = 12$ cm (solid curve). The relatively shorter pulse duration at $\Delta z = 12$ cm is the result of plasma defocusing of the trailing edge of the laser. Figure 9(b) plots the corresponding radial Poynting flux of the EMP versus time at radial position $r = 225$ μm. The Poynting flux is peaked in a region behind the driving laser pulse and has a duration that is of the order $\sim 1/\nu_e$. Note that the flux at $\Delta z = 10$ cm is directed radially outward while at $\Delta z = 12$ cm, it is outward just behind the laser pulse and then reverses direction. Figure 9(c) plots the frequency distribution of the two curves shown in Fig. 9(b). The frequency distribution

$$\psi_r(r_0, \omega) \equiv \frac{\Delta\omega}{\sqrt{2\pi}} \int_{-\infty}^{\infty} I_r(r_0, t)e^{i\omega t} dt, \quad (20)$$

has units of intensity and represents the intensity contained within a frequency band $\Delta\omega$, which, for a laboratory experiment, is typically the resolution of the detector used to measure the EMP. In this case, $\Delta\omega/2\pi \sim 1$ THz is the smallest frequency interval that can be resolved by the simulation grid size. The EMP spectrum at $\Delta z = 10$ cm is peaked near zero frequency and is broadband with a width of ~ 10 THz. At

$\Delta z = 10$ cm, the maximum electron collision frequency ν_e $\sim 6 \times 10^{13}$ s^{-1}. At $\Delta z = 12$ cm, the spectrum is broader and a local maximum at a frequency of ~ 2 THz is apparent. The peak plasma frequency varies from ~ 13 to ~ 12 THz over the 2 cm of propagation shown in the plots. Note that there is no distinct feature in the EMP spectrum at the plasma frequency or any of its harmonics.

The total energy radiated in the radial direction during the entire simulation is found to be ~ 50 pJ, which corresponds to an efficiency of $\sim 5 \times 10^{-9}$. Here, efficiency is defined as the ratio of the radiated EMP energy to the laser energy. This is consistent with analytical estimates of the efficiency found in Ref. 48.

VII. SUMMARY

The propagation of ultra-short, intense laser pulses in air involves a broad range of linear and nonlinear processes, many of which have been discussed here. Coupled nonlinear propagation equations which describe the spatial and temporal evolution of the laser envelope have been presented. Simulations show that, consistent with experimental observations, the filamentation process can be strongly dependent on pulse length as a result of the time dependence of the nonlinear refractive index.

An approximate condition for guiding an optical/plasma filament is derived. The dynamic guiding and white light generation from a short pulse is modeled more precisely using the full-scale simulation. Self-guiding of a ~ 100 fs pulse over 10 Rayleigh lengths and spectral broadening from ~ 1.3 μm to the optical range is demonstrated.

The effects of atmospheric turbulence on the nonlinear self-focusing of a laser pulse have been investigated numerically. A particular example was considered in which a chirped pulse was focused at a range of ~ 0.4 km in turbulent and nonturbulent air. It was shown that moderate levels of turbulence can significantly affect the position of the focal point, but that a well defined focus is still achievable.

Finally, the generation of EMP from the propagation of an ionizing ultra-short pulse in air has been analyzed and a recent EMP generation experiment has been simulated. It is found that the efficiency of EMP generation is extremely low. The duration of the EMP is determined by the pulse duration and collision frequency and the resulting spectrum is broadband (tens of THz) with no distinctive feature at the plasma frequency.

[1] A. Braun, G. Korn, X. Liu, D. Du, J. Squier, and G. Mourou, Opt. Lett. **20**, 73 (1995).

[2] E. T. Nibbering, P. F. Curley, G. Grillon, B. S. Prade, M. A. Franco, F. Salin, and A. Mysyrowicz, Opt. Lett. **21**, 1 (1996).

[3] O. G. Kosareva, V. P. Kandidov, A. Brodeur, C. Y. Chien, and S. L. Chin, Opt. Lett. **22**, 1332 (1997).

[4] L. Woste, C. Wedekind, H. Wille, P. Rairoux, B. Stein, S. Nikolov, Ch. Werner, St. Niedermeier, F. Ronneberger, H. Schillinger, and R. Sauerbrey, Laser Optoelektron. **29**, 51 (1997).

[5] B. La Fontaine, F. Vidal, Z. Jiang, C. Y. Chien, D. Comtois, A. Desparois, T. W. Johnston, J.-C. Kieffer, H. Pepin, and H. P. Mercure, Phys. Plasmas **6**, 1615 (1999).

[6] S. Tzortzakis, L. Berge, A. Couairon, M. Franco, B. Prade, and A. Mysyrowicz, Phys. Rev. Lett. **86**, 5470 (2001); A. Couairon, S. Tzortzakis, L. Berge, M. Franco, B. Prade, and A. Mysyrowicz, J. Opt. Soc. Am. B **19**, 1117 (2002).

[7] C. Y. Chien, B. La Fontaine, A. Desparois, Z. Jiang, T. W. Johnston, J.-C. Kieffer, H. Pepin, F. Vidal, and H. P. Mercure, Opt. Lett. **25**, 578 (2000).

[8] J. Kasparian, R. Sauerbrey, D. Mondelain, S. Niedermeier, J. Yu, J.-P. Wolf, Y.-B. Andre, M. Franco, B. Prade, S. Tzortzakis, A. Mysyrowicz, M. Rodriguez, H. Wille, and L. Woste, Opt. Lett. **25**, 1397 (2000).

[9] J. Yu, D. Mondelain, G. Ange, R. Volk, S. Niedermeier, J. P. Wolf, J. Kasparian, and R. Sauerbrey, Opt. Lett. **26**, 533 (2001).

[10] X. M. Zhao, J.-C. Diels, C. Y. Wang, and J. M. Elizondo, IEEE J. Quantum Electron. **31**, 599 (1995).

[11] H. Schillinger and R. Sauerbrey, Appl. Phys. B: Lasers Opt. **68**, 753 (1999).

[12] S. Tzortzakis, M. A. Franco, Y.-B. Andre, A. Chiron, B. Lamouroux, B. S. Prade, and A. Mysyrowicz, Phys. Rev. E **60**, R3505 (1999).

[13] D. Comtois, C. Y. Chien, A. Desparois, F. Genin, G. Jarry, T. W. Johnston, J.-C. Kieffer, B. La Fontaine, F. Martin, R. Mawassi, H. Pepin, F. A. M. Rizk, F. Vidal, P. Couture, H. P. Mercure, C. Potvin, A. Bondiou-Clergerie, and I. Gallimberti, Appl. Phys. Lett. **76**, 819 (2000).

[14] H. D. Ladouceur, A. P. Baronavski, D. Lohrmann, P. W. Grounds, and P. G. Girardi, Opt. Commun. **189**, 107 (2001).

[15] A. Ting, D. Gordon, D. Kaganovich, E. Briscoe, C. Manka, J. Peñano, P. Sprangle, B. Hafizi, and R. Hubbard, "Experiments on the propagation and filamentation of ultrashort intense laser pulses in air," J. Directed Energy (to be published).

[16] A. Proulx, A. Talebpour, S. Petit, and S. L. Chin, Opt. Commun. **174**, 305 (2000).

[17] S. Tzortzakis, G. Méchain, G. Patalano, Y. B. André, B. Prade, M. Franco, A. Mysyrowicz, J. M. Munier, M. Gheudin, G. Beaudin, and P. Encrenaz, Opt. Lett. **27**, 1944 (2002).

[18] J. Kasparian, M. Rodriguez, G. Mejean, J. Yu, E. Salmon, H. Wille, R. Bourayou, S. Frey, Y.-B. Andre, A. Mysyrowicz, R. Sauerbrey, J.-P. Wolfe, and L. Woste, Science **301**, 61 (2003).

[19] M. D. Feit and J. A. Fleck, Appl. Phys. Lett. **24**, 169 (1974).

[20] P. Sprangle, E. Esarey, and J. Krall, Phys. Rev. E **54**, 4211 (1996).

[21] A. Brodeur, C. Y. Chien, F. A. Ilkov, S. L. Chin, O. G. Kosareva, and V. P. Kandidov, Opt. Lett. **22**, 304 (1997).

[22] H. R. Lange, G. Grillon, J.-F. Ripoche, M. A. Franco, B. Lamouroux, B. S. Prade, A. Mysyrowicz, E. T. J. Nibbering, and A. Chiron, Opt. Lett. **23**, 120 (1998).

[23] N. Akozbek, M. Scalora, C. M. Bowden, and S. L. Chin, Opt. Commun. **191**, 353 (2001); N. Akozbek, C. M. Bowden, A. Talebpour, and S. L. Chin, Phys. Rev. E **61**, 4540 (2000).

[24] M. Mlejnek, E. M. Wright, and J. V. Moloney, Opt. Lett. **23**, 382 (1998); Phys. Rev. E **58**, 4903 (1998); Opt. Express **4**, 223 (1999); M. Mlejnek, M. Kolesik, J. V. Moloney, and E. M. Wright, Phys. Rev. Lett. **83**, 2938 (1999).

[25] J. Kasparian, R. Sauerbrey, and S. L. Chin, Appl. Phys. B: Lasers Opt. **71**, 877 (2000).

[26] A. Couairon and L. Berge, Phys. Plasmas **7**, 193 (2000).

[27] E. Esarey, G. Joyce, and P. Sprangle, Phys. Rev. A **44**, 3908 (1991); P. Sprangle and E. Esarey, Phys. Fluids B **4**, 2241 (1992).

[28] M. Henesian, C. D. Swift, and J. R. Murray, Opt. Lett. **10**, 565 (1985).

[29] P. B. Corkum, C. Rolland, and T. Srinivasan-Rao, Phys. Rev. Lett. **57**, 2268 (1986); P. B. Corkum and C. Rolland, IEEE J. Quantum Electron. **25**, 2634 (1989).

[30] G. S. McDonald, G. H. C. New, L. L. Losev, and A. P. Lutsenko, J. Phys. B **30**, L719 (1997).

[31] A. Brodeur and S. L. Chin, J. Opt. Soc. Am. B **16**, 637 (1999).

[32] C. A. Kapetanakos, B. Hafizi, H. M. Milchberg, P. Sprangle, R. F. Hubbard, and A. Ting, IEEE J. Quantum Electron. **35**, 565 (1999); C. A. Kapetanakos, B. Hafizi, P. Sprangle, R. F. Hubbard, and A. Ting, *ibid.* **37**, 641 (2001).

[33] P. Sprangle, J. R. Peñano, and B. Hafizi, Phys. Rev. E **66**, 046418 (2002).

[34]J. R. Ackerhalt and P. Milonni, Phys. Rev. A **33**, 3185 (1986); A. P. Hickman and W. K. Bischel, *ibid.* **37**, 2516 (1988).

[35]J. R. Peñano, P. Sprangle, P. Serafim, B. Hafizi, and A. Ting, Phys. Rev. E **68**, 056502 (2003).

[36]A. Talebpour, J. Yang, and S. L. Chin, Opt. Commun. **163**, 29 (1999).

[37]B. Hafizi, P. Sprangle, J. R. Peñano, and D. F. Gordon, Phys. Rev. E **67**, 056407 (2003).

[38]H. G. Muller, P. Agostini, and G. Petite, in *Atoms in Intense Laser Fields*, edited by M. Gavrilla (Academic, San Diego, 1992).

[39]P. B. Corkum, N. H. Burnete, and F. Brunel, Phys. Rev. Lett. **62**, 1259 (1989).

[40]P. Sprangle, J. R. Peñano, A. Ting, B. Hafizi, and D. F. Gordon, J. Directed Energy **1**, 73 (2003).

[41]V. I. Bespalov and V. I. Talanov, JETP Lett. **3**, 307 (1966).

[42]E. Nibbering, G. Grillon, M. Franco, B. Prade, and A. Mysyrowicz, J. Opt. Soc. Am. B **14**, 650 (1997); J.-F. Ripoche, G. Grillon, B. Prade, M. Franco, E. Nibbering, R. Lange, and A. Mysyrowicz, Opt. Commun. **135**, 310 (1997).

[43]A. Brodeur, C. Y. Chien, F. A. Ilkov, S. L. Chin, O. G. Kosareva, and V. P. Kandidov, Opt. Lett. **22**, 304 (1997).

[44]P. Sprangle and B. Hafizi, Phys. Plasmas **6**, 1683 (1999).

[45]P. Sprangle, A. Ting, and C. M. Tang, Phys. Rev. A **36**, 2773 (1987).

[46]J. A. Fleck, J. R. Morris, and M. D. Feit, Appl. Phys. **10**, 129 (1976).

[47]M. E. Thomas and D. D. Duncan, in *The Infrared and Electron-Optical Systems Handbook*, Vol. 2, edited by F. G. Smith, Environmental Research Institute of Michigan, Ann Arbor (MI and SPIE Optical Engineering Press, Bellingham, WA, 1993).

[48]P. Sprangle, J. R. Peñano, B. Hafizi, and C. A. Kapetanakos, NRL Memorandum NRL/MR/6790-03-8693.

[49]C. C. Cheng, E. M. Wright, and J. V. Moloney, Phys. Rev. Lett. **87**, 213001 (2001); **89**, 139302 (2002).

[50]G. Shvets, I. Kaganovich, and E. Startsev, Phys. Rev. Lett. **89**, 139301 (2002).